Molecular Cell
Article

Structural Mechanism of Substrate RNA Recruitment in H/ACA RNA-Guided Pseudouridine Synthase

Jingqi Duan,[1,2] Ling Li,[2] Jing Lu,[2,3] Wei Wang,[2,3] and Keqiong Ye[2,*]
[1]College of Life Sciences, Peking University, Beijing 100871, China
[2]National Institute of Biological Sciences, Beijing 102206, China
[3]Graduate Program in Chinese Academy of Medical Sciences and Peking Union Medical College, Beijing 100730, China
*Correspondence: yekeqiong@nibs.ac.cn
DOI 10.1016/j.molcel.2009.05.005

SUMMARY

H/ACA RNAs form ribonucleoprotein complex (RNP) with proteins Cbf5, Nop10, L7Ae, and Gar1 and guide site-specific conversion of uridine into pseudouridine in cellular RNAs. The crystal structures of H/ACA RNP with substrate bound at the active site cleft reveal that the substrate is recruited through sequence-specific pairing with guide RNA and essential protein contacts. Substrate binding leads to a reorganization of a preset pseudouridylation pocket and an adaptive movement of the PUA domain and the lower stem of the H/ACA RNA. Moreover, a thumb loop flips from the Gar1-bound state in the substrate-free RNP structure to tightly associate with the substrate. Mutagenesis and enzyme kinetics analysis suggest a critical role of Gar1 and the thumb in substrate turnover, particularly in product release. Comparison with tRNA Ψ55 synthase TruB reveals the structural conservation and adaptation between an RNA-guided and stand-alone pseudouridine synthase and provides insight into the guide-independent activity of Cbf5.

INTRODUCTION

Pseudouridine (Ψ) is the most frequently modified nucleotide in structured RNAs, including transfer, ribosomal, and spliceosomal small nuclear RNAs. Certain Ψs have been shown to be important for the function of ribosome and spliceosome (King et al., 2003; Ejby et al., 2007; Piekna-Przybylska et al., 2008; Yu et al., 1998; Yang et al., 2005).

Ψ is posttranscriptionally converted from uridine (U) at specific positions in RNA by Ψ synthases (ΨSs) (Hamma and Ferre-D'Amare, 2006). Due to the vast diversity in substrate structure and sequence, there are a large number of ΨSs, with each modifying one or several specific Us. Currently, ΨSs fall into six sequence families: TruA, TruB, RluA, RsuA, TruD, and Pus10 (Koonin, 1996; Hamma and Ferre-D'Amare, 2006; Roovers et al., 2006). All ΨSs except for H/ACA RNA-guided ΨSs are single-polypeptide stand-alone enzymes. Structures of TruB, RluA, and TruA, in complex with substrate RNA, have showed that they recognize the particular structure that a substrate adopts (Hoang and Ferre-D'Amare, 2001; Pan et al., 2003; Phannachet and Huang, 2004; Hoang et al., 2006; Hur and Stroud, 2007). In contrast, H/ACA RNA-guided ΨSs are composed of four proteins—Cbf5 (dyskerin in humans), Nop10, L7Ae (Nhp2 in eukaryotes), and Gar1—and a distinct H/ACA guide RNA, and they recognize substrates via the guide RNA (Kiss, 2001; Meier, 2005; Reichow et al., 2007). The recognition by H/ACA guide RNA depends only on the sequence, not structure, of the substrate RNA. Any preformed structure of substrate must be unfolded before association with the guide RNA. In eukaryotic and archaeal organisms, abundant Ψs in rRNAs and snRNAs are modified in this unique RNA-guided manner.

In the majority of eukaryotes, H/ACA RNAs fold into a consensus hairpin-hinge-hairpin-tail structure, which contains a conserved sequence motif H box in the hinge region (ANANNA, in which N is any nucleotide) and an ACA box in the 3′ tail located three nucleotides (nt) away from the 3′ end (Balakin et al., 1996; Ganot et al., 1997b). Each hairpin can harbor a large internal loop, termed the pseudouridylation (ψ) pocket. This pocket is responsible for base pairing with the substrate RNA on either side of a dinucleotide "UN," in which U is the target to be modified (Ganot et al., 1997a; Ni et al., 1997). H/ACA RNAs in archaea contain a kink-turn structural motif in the upper stem of each hairpin, with a total of one to three hairpins (Tang et al., 2002; Rozhdestvensky et al., 2003).

H/ACA RNP assembled from archaeal Cbf5, Nop10, L7Ae, and Gar1 and an H/ACA guide RNA displayed site-specific pseudouridylation activity (Baker et al., 2005; Charpentier et al., 2005). Cbf5 catalyzes the modification and shares significant sequence similarity with TruB, which is responsible for generating Ψ55 in tRNA. The other three proteins are essential for optimal activity (Baker et al., 2005; Charpentier et al., 2005). The recent structural determination of archaeal H/ACA complex has provided great insight into its organization and mechanism of action (Ye, 2007; Reichow et al., 2007). Cbf5 is composed of a PUA domain and a catalytic domain, which is further divided into subdomains D1 and D2 by the active site cleft. The small protein Nop10, partially unstructured in isolation (Hamma et al., 2005; Khanna et al., 2006; Reichow and Varani, 2008), associates tightly with the catalytic domain of Cbf5 (Hamma et al., 2005; Manival et al., 2006; Rashid et al., 2006), and Gar1 binds independently at Cbf5 D2 (Rashid et al., 2006). We previously determined the structure of a fully assembled H/ACA RNP in which a single hairpin H/ACA RNA adopts an extended conformation and associates with Cbf5, Nop10, and L7Ae (Li and Ye, 2006). The organization of RNP places the guide regions in the vicinity of the active site cleft. Although Gar1 does not bind the

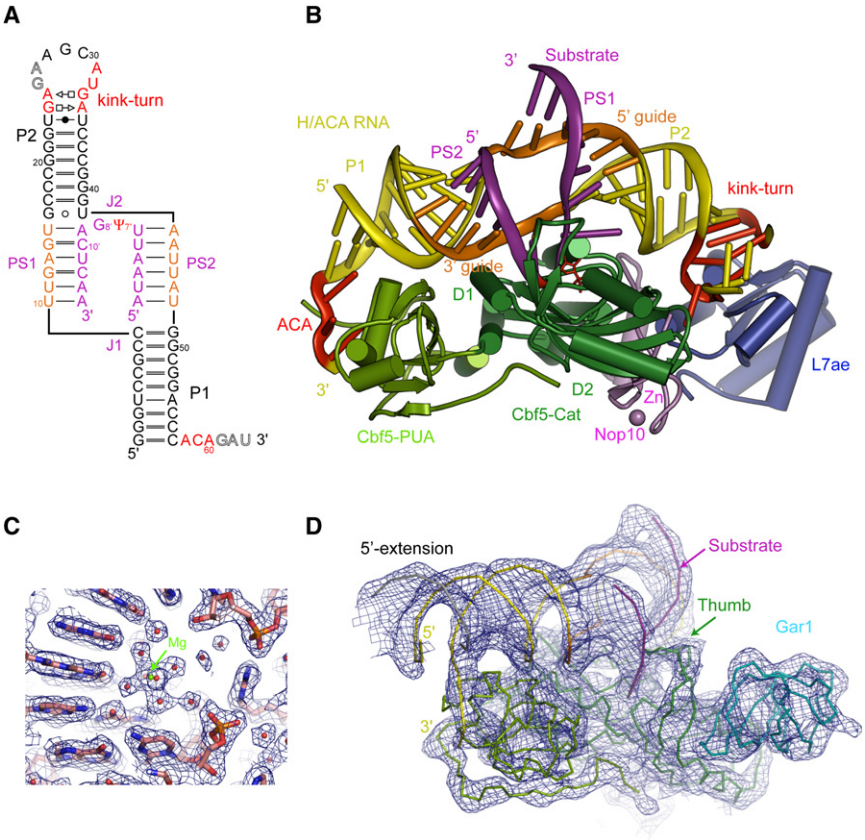

Figure 1. Overview of Substrate-Bound H/ACA RNP Structures

(A) Secondary structure of H/ACA RNA1 with substrate RNA bound at the pseudouridylation pocket. The lower (P1) and upper (P2) stems, substrate-guide helices PS1 and PS2, and the lower (J1) and upper (J2) three-way junctions are indicated. Base pair symbols are depicted according to a previous rule (Leontis and Westhof, 2001). Hollow letters represent disordered residues in the Gar-minus structure. Prime denotes substrate RNA.

(B) Ribbon representation of the substrate-bound Gar1-minus H/ACA RNP structure, showing Cbf5 PUA domain in light green; Cbf5 catalytic (Cat) domain in dark green; Nop10 in magenta; L7Ae in blue; substrate RNA in purple; guide sequences in orange; the ACA motif, kink-turn motif, and target nucleotide in red; and the remainder of the H/ACA RNA in yellow. The target nucleotide is shown as sticks.

(C) SIGMAA-weighted $2F_o - F_c$ electron density map of the Gar1-minus complex. The 2.1 Å map is contoured at 1 σ. The refined structure is shown as sticks with carbon atoms colored in pink, oxygen in red, nitrogen in blue, phosphorus in orange, and magnesium in green.

(D) The substrate-bound full-complex structure represented as Cα or P traces. The solvent-modified 5 Å electron density map contoured at 1 σ is indicated. Gar1 is colored cyan, and other parts are color coded as in Figure 1B. A symmetry-related molecule, colored in gray, forms a self-duplex with the 5′ extension of H/ACA RNA2.

H/ACA RNA, it sequesters a thumb loop of Cbf5. Based on the position of a modeled substrate, Gar1 was hypothesized to regulate substrate turnover by controlling the thumb position.

To understand how substrate is recruited by H/ACA guide RNA, two NMR structures of a substrate-guide RNA complex and a crystal structure of a substrate-bound H/ACA RNP were determined (Wu and Feigon, 2007; Jin et al., 2007; Liang et al., 2007; Li, 2008). However, the latter complex did not include L7Ae, and consequently, the substrate RNA was not positioned at the active site. The substrate RNA has been modeled based on TruB-RNA interaction (Li and Ye, 2006). Even with these advances, the fundamental question of how H/ACA RNA recognizes its substrate and leads the target uridine to the active site for modification remains unresolved. More recently, archaeal Cbf5 was found to catalyze the formation of Ψ55 in tRNA in the absence of guide RNA (Roovers et al., 2006). It is puzzling how Cbf5 could assume a dual function in both guide-dependent and guide-independent manners. To address these questions, we characterize the structure of H/ACA RNP with substrate loaded at the active site and investigate the mechanism controlling substrate loading and release by mutagenesis and enzyme kinetics analysis.

RESULTS

Crystallization and Structure Determination

A 14 nt substrate RNA was designed to bind the ψ pocket of an H/ACA RNA species RNA1 (Figure 1A). The substrate contains a 5-fluorouridine (f^5U) in place of U at the site of modification. We have attempted to crystallize the substrate with fully assembled H/ACA RNPs containing all four RNP proteins—Cbf5, Nop10, L7Ae, and Gar1—from *Pyrococcus furiosus*, in addition to an H/ACA guide RNA. To promote diverse crystal packing, we modified the RNA1 construct by attaching palindromic sequences 7–10 nt in length at either the 5′ or 3′ end. These extensions were expected to form a self-pairing duplex between neighboring RNA molecules in crystal, promoting and modulating crystallographic RNA-RNA interactions. Substrate-bound RNPs assembled from either RNA1 or two other 5′ derivatives grew poor-quality crystals. The structure that we report here was obtained from an RNA2 species, which has an 8 nt extension at the 5′ end of RNA1 (5′-GGCUGCCU-3′; the self-pairing region is underlined). The extension formed a 7 base pair (bp) duplex in the crystal, as expected (Figure 1D). The strategy of engineering a self-pairing RNA element may be applicable for other types of RNP/RNA crystallization, although it did not yield a high-resolution crystal in our case. This approach is similar to the use of sticky ends to promote end-to-end stacking of helices in crystal (Wedekind and McKay, 2000).

Meanwhile, high-quality crystals were obtained from a partially assembled five-component complex that used the RNA1 construct but omitted the Gar1 protein (hereafter called the Gar1-minus complex). The structure was determined by molecular replacement and refined to 2.1 Å with a free R value of 0.22. Its electron density map is shown in Figure 1C, highlighting

Table 1. Data Collection and Refinement Statistics

Data Collection		
Crystal	Gar1-minus complex	Full complex
PDB ID	3HAX	3HAY
Space group	$P2_12_12$	$P6_422$
Unit cell dimensions a, b, c (Å)	187.809, 63.696, 83.848	189.518, 189.518, 279.045
X-ray source	SPring-8/BL41XU	SPring-8/BL41XU
Wavelength (Å)	1.0000	1.0000
[a]Resolution (Å)	50–2.09 (2.16–2.09)	50–5.0 (5.18–5.00)
Total observations	226,059	136,728
Unique reflections	57,734	13,408
Redundancy	3.9	10.2
Completeness (%)	99.6 (99.9)	99.5 (99.8)
Mean I/σ	13.7 (2.7)	34.4 (4.7)
[b]R_{merge}	0.114 (0.515)	0.082 (0.481)
Refinement Statistics		
Resolution limits (Å)	20–2.11 (2.16–2.11)	20–5.0 (5.11–5.0)
Number of reflections	54,667	12,531
Completeness (%)	98.19 (79.3)	99.98 (98.67)
Number of atoms	5960	6327
[c]R_{work}	0.203 (0.233)	0.323 (0.379)
[d]R_{free}	0.220 (0.252)	0.367 (0.509)
Rmsd bonds (Å)	0.006	0.007
Rmsd angles (°)	0.959	0.971
[e]Ramachandran statistics (%)	95.1, 4.4, 0.2, 0.2	87.5, 11.7, 0.6, 0.2

[a] Data for the outermost shell are given in parentheses.
[b] $R_{merge} = \Sigma_{hkl}\Sigma_i |I_i - < I > |/\Sigma_{hkl}\Sigma_i I_i$, wherein I_i is the i^{th} measurement of diffraction intensity I and $< I >$ is the average of all measurements of I.
[c] $R_{work} = \Sigma_{hkl}||F_o| - |F_c||/\Sigma_{hkl}|F_o|$, wherein F_o and F_c are the observed and calculated structure factor amplitudes.
[d] R_{free} is the same as R_{work} calculated on 5% of the reflections not used in refinement.
[e] Residues in the most favored, additionally allowed, generously allowed, and disallowed regions of the Ramachandran diagram.

a magnesium hexahydrate ion bound at the major groove of a RNA helix. The Gar1-minus structure was then used to build a 5 Å model for the full complex. The data collection and refinement statistics for the two structures are shown in Table 1.

Overall Structure

In the substrate-bound Gar1-minus complex structure (Figure 1B and Movie S1 available online), the H/ACA RNA, except for its ψ pocket, associates with Cbf5, Nop10, and L7Ae in essentially the same way as seen in the free complex (Li and Ye, 2006). The upper stem (P2) interacts with L7Ae, Nop10, and the Cbf5 D1 subdomain, whereas the lower stem (P1) and 3′ ACA tail are anchored at the PUA domain of Cbf5. The substrate RNA associates with the ψ pocket from the active site cleft side and adopts a U-shaped structure that is aligned vertically to the protein surface. In addition, the substrate is locked in place by extensive protein contacts, particularly from the thumb loop of Cbf5. The target nucleotide f^5U is buried at the active site cleft and has been converted into the product (see below). Due to the placement of the converted product in the active site, in addition to the extensive association between Cbf5 and substrate, we believe that the Gar1-minus structure faithfully represents an active conformation of the enzyme. These features were absent in the previous structure of substrate-bound RNP lacking L7Ae (Liang et al., 2007).

The structure of substrate-bound full complex (Figure 1D) shows that Gar1 associates with Cbf5 D2 at the same position as in the free RNP structure. Gar1 does not contact either the H/ACA guide RNA or substrate RNA. The rest of complex, including the substrate-guide helices and the thumb, assumes the same organization as in the Gar1-minus complex. The similarity between the two substrate-bound RNP structures suggests that Gar1 does not directly contribute to the conformation of loaded substrate.

Substrate-Bound ψ Pocket

Association of the substrate with the 5′ and 3′ guides leads to the formation of two 6 bp helices, PS1 and PS2, at the ψ pocket (Figures 1A and 2A). PS1 refers to the helix formed by the 5′ guide and the 3′ arm of substrate, and PS2 refers to the helix formed by the 3′ guide and the 5′ arm of substrate. The two substrate-guide helices run in parallel, with their major grooves facing each other; however, there are no interhelix interactions between them. We observed five hydrated magnesium ions bound to the RNA; three bind in the major groove of the P1 and P2 stems, and two mediate crystal packing (Figure 2A).

The two guide-substrate helices are connected to the lower and upper stems via the lower (J1) and upper (J2) three-way junctions, respectively (Figure 2A). At the J1 junction, helix PS2 stacks coaxially over P1, forming an ideal pseudocontinuous helix. The nonstacked helices P1 and PS1 are covalently linked, inducing a sharp kink in the phosphate backbone between C9 and U10. At the J2 junction, helix PS1 coaxially stacks over P2 but with an extra twist. The base pairs U15•A9′ and G16•U42 at the junction of PS1 and P2 are related by a helical twist of 55°, in contrast with a normal twist of 32° found in A-form duplexes. This results in A9′ and U42 being unstacked from each other. The phosphate backbone between U42 and A43, at the junction of nonstacked helices P2 and PS2, is also abruptly bent. The J1 and J2 junctions are similar in topology, except that PS1 and PS2 are covalently connected by the "UN" dinucleotide in J2 and not with each other in J1.

All substrate-bound ψ pockets characterized so far, although variable in their exact conformation, display similar topological features (Jin et al., 2007; Wu and Feigon, 2007; Liang et al., 2007). These features include a U-shaped conformation of the bound substrate, coaxial stacking between substrate-guide helices and P1/P2 stems, and kinks in the phosphate backbone of the H/ACA RNA linking the nonstacked helices at each three-way junction. The ψ pocket, basically a long two-stranded loop embedded in a duplex, appears to have the intrinsic capacity to mold associated RNA into such an architecture.

RNA-Protein Interaction

The P1-PS2 helical stack employs two successive minor grooves to interact with the PUA and catalytic domain of Cbf5,

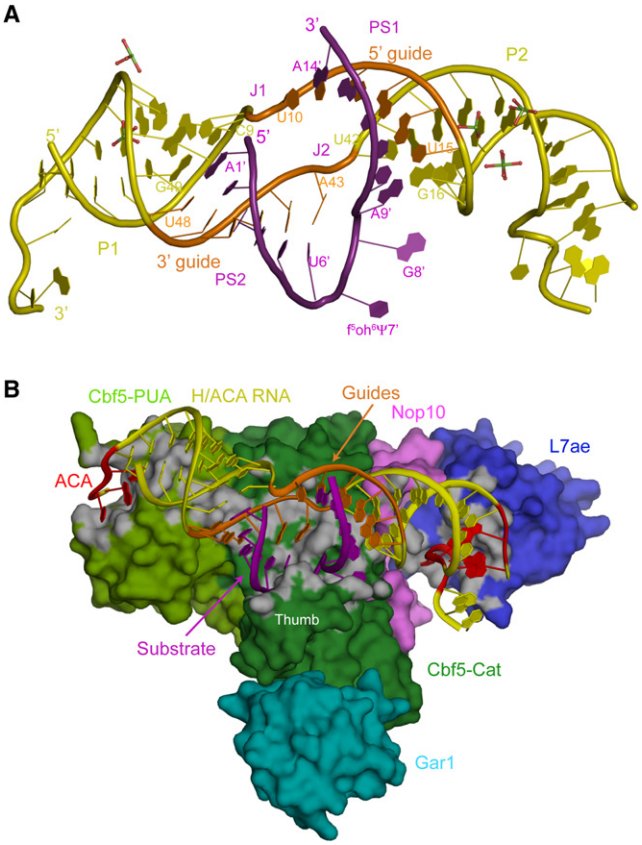

Figure 2. Structure and RNP Assembly of Substrate-Bound H/ACA RNA

(A) Structure of substrate-bound H/ACA RNA. Hydrated Mg ions are shown as sticks with Mg colored green and water red.

(B) RNA-binding surface in substrate-bound H/ACA RNP. Shown are the Gar1-minus RNP structure with Gar1 modeled according to its position in the full complex. RNAs are represented as ribbons and planes, and proteins are represented as surfaces. Individual parts are color coded as in Figure 1B. The RNA-binding surface (within 4 Å of RNA) is colored in gray.

respectively, with the intervening major groove facing the border of the two domains (Figures 1B and 2B). The P1 stem and the ACA motif bind at the PUA domain with the same set of interactions as in the substrate-free structure, whereas the association of PS2 involves a new set of interactions that are not present when the ψ pocket is empty. The guide strand of PS2 binds at the floor of Cbf5 D1 with direct and water-mediated interactions (Figures 3A and 3D). The terminal base of the PS2 helix in the guide strand, A43, is capped by an invariant histidine H63, which further interacts with substrate RNA and residue H80. The substrate strand in PS2 is bound mainly by the thumb (Figure 3B), as described below. The spatial arrangement of PS2 and PS1 in the RNP precisely places the target uridine inside of the active site cleft. In contrast with extensive interactions directed to the PS2 helix and UN dinucleotide, the PS1 helix is nearly free of protein interaction (Figure 3D). None of the protein interaction recognizes the specific sequence feature of the substrate, except for the target nucleotide, consistent with the fact that only base pairing with guide RNA determines substrate specificity.

The ACA motif and the target nucleotide to be modified are placed at opposing ends of the P1-PS2 helical stack and are tightly bound by the PUA domain and the active site cleft, respectively. Due to the rigidity of the P1-PS2 helical structure and the extensive protein interaction along one face of the P1-PS2 helical stack, a large insertion and deletion in the P1-PS2 helical stack would be detrimental to the precise assembly of substrate. These structural constraints lead to a conservation in the overall length of the jointed P1-PS2 helical stack, which encompasses the distance between the ACA motif and the target U (Ganot et al., 1997a; Ni et al., 1997). In our structure, the P1-PS2 helical stack is fully paired and spans 15 bp. However, the joint helical stack can vary between 14 and 16 bp in length and occasionally contains an unpaired region (Ganot et al., 1997a; Ni et al., 1997). Small variations in the P1-PS2 length could be tolerated due to the plasticity of the connection between the PUA and catalytic domain of Cbf5 (see below). The junction region between P1 and PS2 is not in contact with Cbf5 and may be suitable for housing these variations. In addition, helix PS1 experiences no structural constraints from protein interaction and appears to be more accommodating to structural variations.

Substrate-Bound Closed Conformation of the Thumb

Structural analysis has shown that two RNA-binding loops, named the forefinger and thumb loops, are often present in ΨSs at the opposite sides of the active site cleft and contribute to substrate-specific recognition (Hamma and Ferre-D'Amare, 2006; Hur and Stroud, 2007). Cbf5, like TruB, has a thumb loop but lacks a forefinger loop. The thumb in Cbf5 is composed of a highly conserved Arg-rich region (residues 140–156) located between strands β7 and β10 (Figures 3B and 3C). Our structures show that the thumb makes intimate contact with the bottom portion of the U-shaped substrate RNA, locking the target nucleotide at the active site cleft (Figure 3B). No interactions occur between the thumb and H/ACA RNA, suggesting that the thumb is dedicated to substrate recruitment. Here, the substrate-bound conformation of the thumb is referred to as the closed state, whereas the Gar-bound state of the thumb in the free RNP structure is referred to as the open state. Substrate binding induces the thumb to switch from the open to closed state. This movement is accompanied by the breaking and reforming of many interactions (Figures 3B and 4A).

The N-terminal segment of the thumb (residues 140–145) is the major region mediating the Gar1 interaction in the open state (Figure 4A). During the open-to-closed state transition, residues 141–145 undergo a hinge-like rotation, resulting in a large movement (18 Å) of L145 Cα (Figure 4A). The segment flips over and interacts with the floor of the Cbf5 D2 subdomain (Figures 3B and 4A). A set of tandem proline residues, P143 and P144, pack against the reorientated aromatic ring of Y182, and the side chain amide group of Q141 forms two closed-state-specific hydrogen bonds with the backbone atoms of Y182. Notably, these intermolecular interactions could occur even in the Cbf5-Nop10-Gar1 protein complex (Rashid et al., 2006), suggesting that they might drive the initial flipping of the thumb when the substrate RNA is not fully in place.

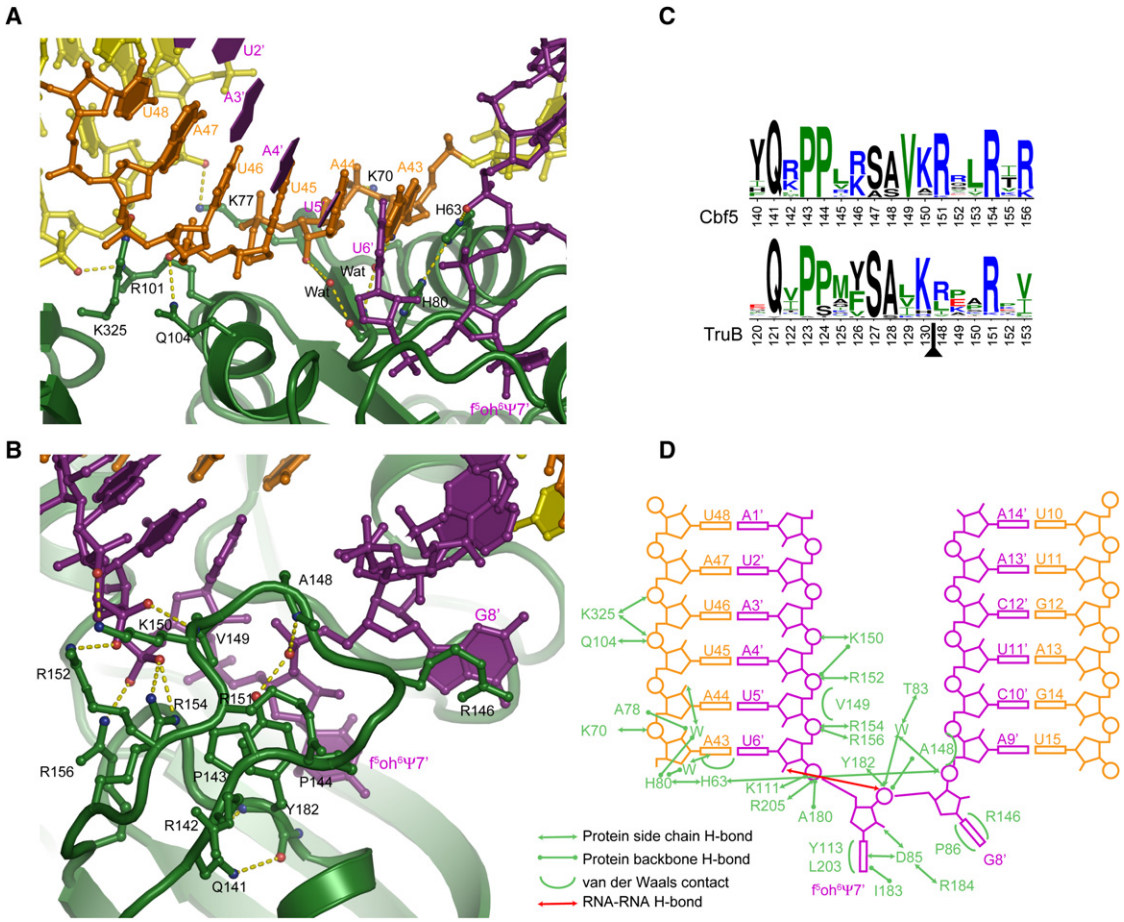

Figure 3. Protein-RNA Interaction in Detail

(A) Interaction between the substrate-guide helix PS2 and the Cbf5 D1 subdomain. For clarity, residues 1′–5′ of the substrate are shown with only base planes, and the thumb is not displayed. Oxygen and nitrogen atoms involved in hydrogen bonding are shown in red and blue, respectively. Dashed lines indicate hydrogen bonds.

(B) Interaction of the thumb in the closed state.

(C) Sequence conservation of the thumb in archaeal Cbf5 (55 sequences) and bacterial TruB (854 sequences), created by WebLogo (Crooks et al., 2004). Corresponding residues in Cbf5 and TruB are aligned based on structural superposition. The bar indicates insertion 2 in TruB. The height of the whole letter stack indicates the sequence conservation at that position, and the height of each letter is proportional to the relative frequency of the amino acid that the letter represents. Hydrophobic residues (L, V, I, W, M, F, P) are green, basic residues (R, K) are red, acidic residues (D, E) are blue, and all other residues are black.

(D) Schematic view of interactions at the substrate-bound ψ pocket.

The rest of the thumb binds its substrate RNA through extensive hydrogen bonding, electrostatic, and van der Waals interactions (Figure 3B). The guanidine group of R146 stacks over the base of G8′, the unpaired nucleotide at 3′ of the target, on the verge of the catalytic cleft. The tip of the thumb (S147, A148, and V149) fits neatly into a complementary space between the 5′ and 3′ arms of substrate. The closeness of the protein-RNA contacts at the tip is manifested by the hydrogen bonds formed between the protein backbone atoms (amide nitrogens for A148 and K150) and the nonbridging phosphate oxygen of the substrate RNA. The exact size and shape of the tip appears be critical because V149 is invariant, whereas A148 and S147 are always alanine or serine in Cbf5 proteins (Figure 3C). Following the tip, a series of basic residues located at one face of the loop (K150, R152, R154, and R156) interact with the phosphate groups of the 5′ arm of substrate RNA.

Substrate Binding-Induced Structural Change

To further illustrate the conformational change on substrate binding, we aligned the structures of the substrate-bound Gar1-minus RNP and free RNP using the catalytic domain of Cbf5 (Figure 4B). The catalytic domains, except the thumb, can be closely aligned with an rmsd of 0.48 Å over 188 paired Cα atoms (0.48 Å/188 Cα). Virtually no movement is detected for Nop10 (0.61 Å/53 Cα), L7Ae (0.71 Å/121 Cα), and the P2 upper stem of H/ACA RNA (0.87 Å/21 P), although these components are not directly aligned. Therefore, the Cbf5 catalytic domain core, Nop10, L7Ae, and the P2 stem constitute a rigid block in the RNP complex. In contrast, the PUA

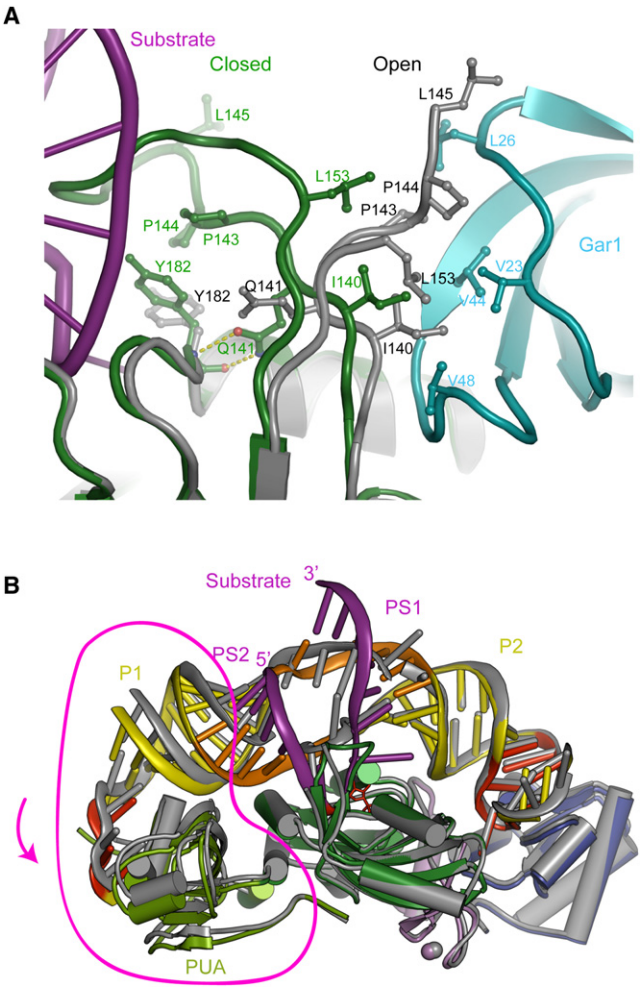

Figure 4. Substrate-Induced Conformation Changes in H/ACA RNP

(A) The closed and open conformation of the thumb. Cbf5 in the substrate-bound and free H/ACA RNP structures are colored green and gray, respectively. Residues involved in protein-protein interactions are shown as balls and sticks.

(B) Structural alignment of substrate-bound and free H/ACA RNPs. The free structure is colored gray and excludes Gar1 for clarity. The arrow indicates the direction of the movement of the PUA domain and the P1 stem.

domain (2.18 Å/108 Cα) and its associated P1 stem (3.23 Å/21 P) are found to undergo a noticeable hinge-like rotation in the direction opposite to where P1 binds; the movement apparently creates more space for substrate binding. However, the PUA-P1 interactions remain intact in the domain movement.

Upon substrate binding, the two guide sequences fold from a loose conformation in the substrate-free RNP into well-ordered helices. The position of each guide shifts only marginally during the transition (Figure 4B) because the P1 and P2 stems to which the two ends of each guide sequence are tethered remain stably associated with the RNP proteins. Hence, the two guides are already placed into the appropriate positions by the flanking stems prior to substrate binding.

Mutagenesis Analysis of the Thumb and Gar1

The structures of substrate-bound and free H/ACA RNP illustrate the dynamic nature of the thumb. Nevertheless, the significance of the thumb adopting the open and closed states and the function of Gar1 remain unclear. Gar1 has been shown to be critical for the full activity of H/ACA RNPs (Baker et al., 2005; Charpentier et al., 2005). Here, we applied structure-directed mutagenesis to the thumb and Gar1 to assess their roles in enzymatic activity (Figure 5). We created a DEL7 mutant by deleting seven residues in the thumb. The thumb contains six arginine residues (R142, R146, R151, R152, R154, and R156), of which four contact the loaded substrate RNA. To evaluate the importance of their involvement in ionic interactions, we replaced each of the six arginine residues with an uncharged glutamine. In addition, we substituted Cbf5 Q141 with an asparagine to disrupt its side-chain interaction with the backbone seen in the closed state. To disturb the thumb-Gar1 interaction in the open state, we mutated a few hydrophobic residues at the binding interface (Figure 4A). We replaced Cbf5 I140, L145, and L153 with glycine, an amino acid with no side chain, and changed Gar1 L26 and V44 to less hydrophobic (L26A, L26G) or charged amino acid residues (V44D). As a control, we changed Gar1 F15 and K56, which are exposed and do not contact Cbf5, to alanine.

These mutations did not disrupt the RNP assembly, as all mutant proteins remained capable of assembling into full RNPs in electrophoretic mobility shift assay (EMSA) (Figure 5A). Using equal amounts of wild-type and mutant full RNPs and Gar1-minus RNP, we assessed their modification activity on a cognate RNA substrate. To detect specifically the target U and its conversion to Ψ, a small amount of the substrate was ^{32}P-labeled at a single site at the 3′ position of the target U. After digesting of substrate into 3′-P mononucleotides, U and Ψ were resolved by thin layer chromatography (TLC). These RNP variants (1 μM) were incubated with ~0.01 μM ^{32}P-labeled substrate and 0, 1, 5, or 20 μM of additional unlabeled substrate. The varied substrate-to-enzyme ratios (S/E) allowed for comparison of the enzymatic activity under single- (S/E = 0.01, 1) and multiple-turnover (S/E = 5, 20) conditions (Figure 5B).

Under single-turnover conditions, the modification by the wild-type enzyme was 91% complete after 10 min in 0.01 μM substrate and 75% complete after 5 min in 1 μM substrate. The reaction rate at single-turnover conditions is consistent with two previous measurements (Charpentier et al., 2005; Gurha et al., 2007) and higher than another measurement (Baker et al., 2005). When the substrate was present at 5 μM, a 5-fold excess over the enzyme, the reaction progress curve displayed a burst phase followed by slower kinetics. Forty one percent, or 2 μM, of the substrate was modified after 5 min. The burst phase in the first 5 min could be ascribed, in part, to the rapid association and modification of the first substrate occurring at the presteady state of reaction. Given that the concentration of active enzyme (1 μM) determines the yield in the presteady state, the presteady-state reaction accounts for about half of the 5 min yield, whereas the remaining half must come from reaction at the steady state. In 20 μM substrate, the presteady-state reaction is not discernible (<5%), and the modification follows pseudo-first-order kinetics. We estimated the turnover rate to be about 0.32 ± 0.02 min^{-1} at the initial steady-state phase of this reaction.

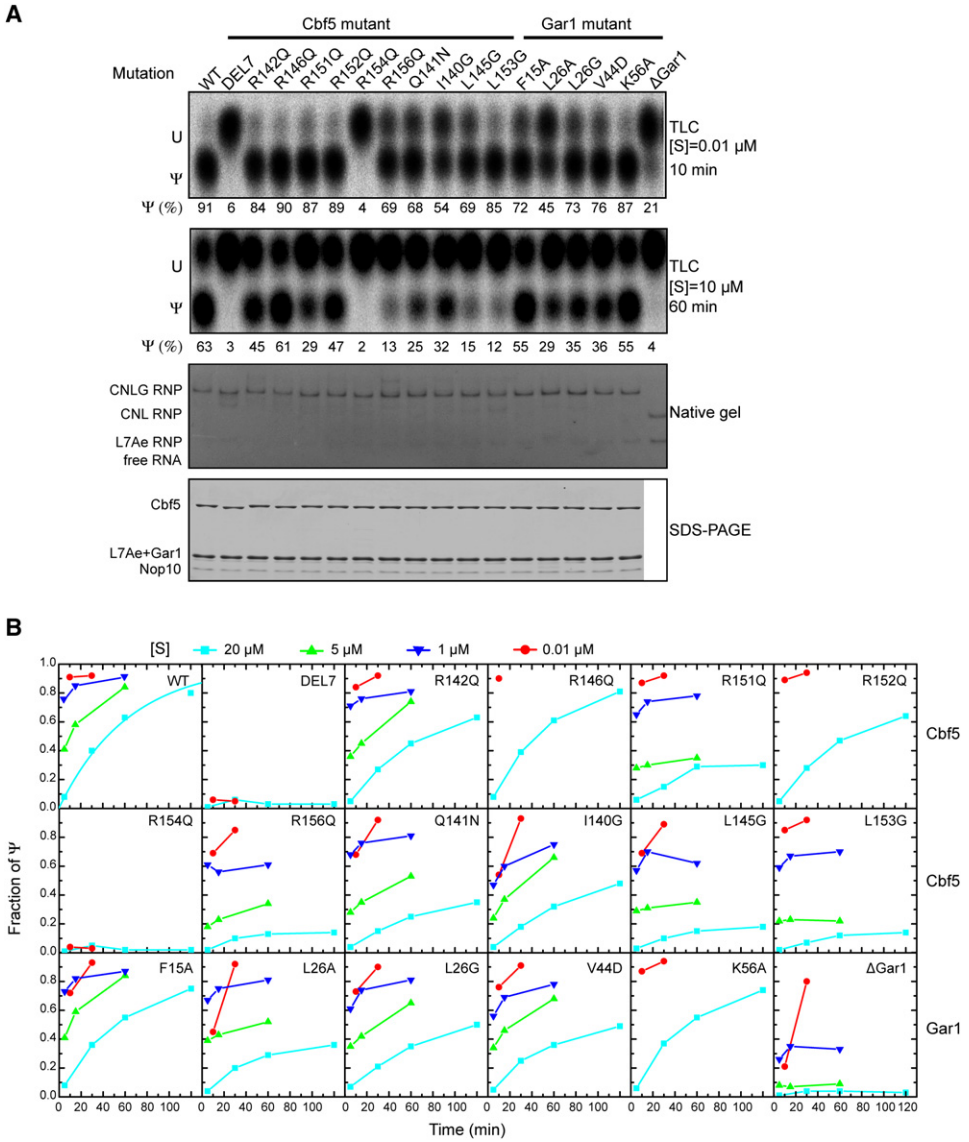

Figure 5. Mutagenesis Analysis of the Thumb and Gar1

(A) Pseudouridylation activity of H/ACA RNP variants. Shown are representative autoradiographs of TLC plates for a 10 min reaction in 0.01 μM substrate (row 1) and a 1 hr reaction in 10 μM substrate (row 2). The percentages of converted Ψ are indicated. The assembled RNP variants were analyzed with an ethidium-bromide-stained native gel (row 3) and a Coomassie-stained SDS-PAGE gel (row 4), showing equal amounts of RNPs and proteins in use. CNGL and CNL stand for the full and Gar1-minus RNP, respectively.

(B) Time course of H/ACA RNP-mediated pseudouridylation. Activities were measured with 1 μM enzyme and 0.01, 1, 5, or 20 μM substrate in 1 M NaCl and 50 mM phosphate (pH 7.0) at 37°C. Some RNP variants with normal or zero activities were not characterized at all four substrate concentrations. For wild-type RNP in 20 μM substrate, the best fit to a single exponential function is shown, whereas all other data are connected by lines.

The complexes assembled by Cbf5 mutants R142Q, R146Q, and R152Q and Gar1 mutants F15A and K56A showed similar or slightly reduced activities relative to wild-type RNP, as judged by their activities in 20 μM substrate. The observed ionic interaction between R152 and substrate appears to have minor influence on the reaction rate. The activity of mutant R146Q was unaffected, consistent with the structural observation that R146 interacts with substrate via stacking rather than electrostatic interactions. The control Gar1 mutants F15A and K56A showed normal activity, as expected. The wild-type activities of these mutants show that our biochemical assays are consistent. Two Cbf5 mutations, DEL7 and R154Q, caused complete loss of activity under all conditions, indicating that both the thumb and residue R154 are required for the substrate to adopt a catalysis-competent conformation.

The remaining single-site mutant RNPs were significantly impaired under multiple-turnover conditions but surprisingly retained substantial activity under single-turnover conditions.

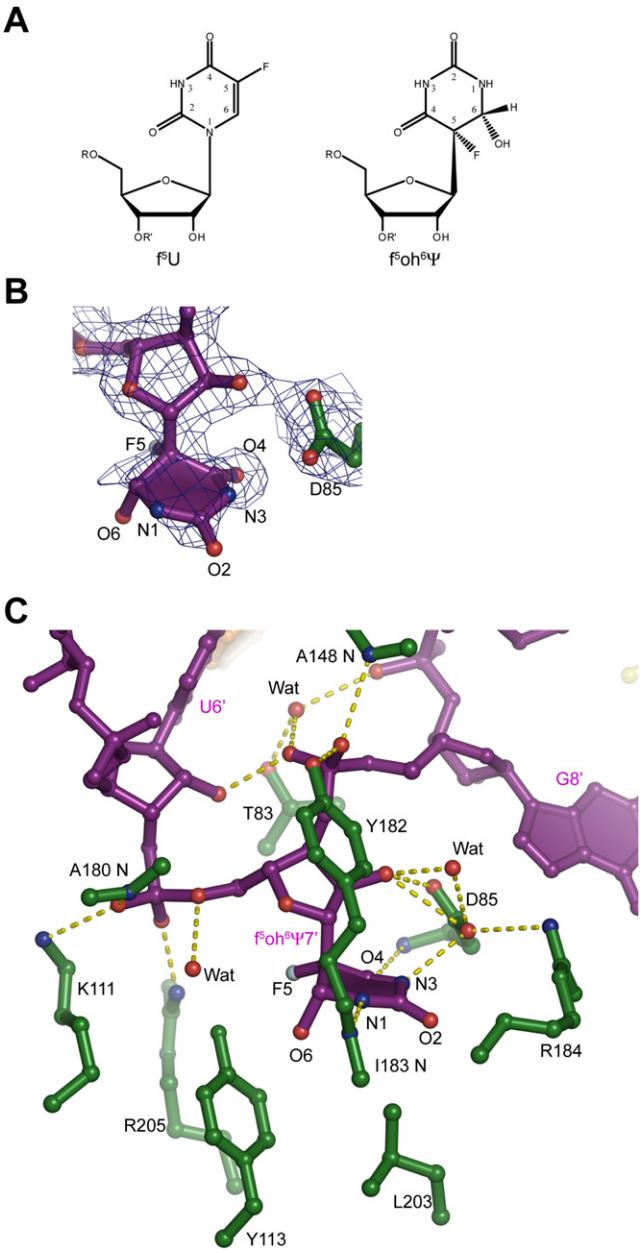

Figure 6. Product of f^5U and the Active Site

(A) Chemical structure of f^5U and $f^5oh^6\Psi$.

(B) The 2.1 Å $2F_o - F_c$ electron density map at the active site, contoured at 1.5 σ. The map was calculated from a model in which the $f^5oh^6\Psi7'$ base was omitted.

(C) Interaction with product $f^5oh^6\Psi$ at the active site.

Using the 60 min yield of wild-type RNP in 20 μM substrate as a reference, the yield decreased to ~50% in Cbf5 mutants R151Q, Q141N, and I140G and Gar1 mutants L26A, L26G, and V44D and to ~25% in Cbf5 mutants R156Q, L145G, and L153G. In contrast, the activities measured under single-turnover conditions in 0.01 and 1 μM substrate were comparable within experimental uncertainty between wild-type and these mutant RNPs. Hence, we can conclude that these mutations primarily reduce the rate of substrate turnover and have less effect on the single-turnover reaction rate.

The modification reaction can be divided into three sequential steps: substrate loading, catalysis, and product release. Under single-turnover conditions, the reaction requires substrate loading and catalysis but does not necessarily require product release. Given that single-turnover reactions were not much inhibited within our detection limits, the substrate loading and catalysis step appear to be less impaired with these mutations. Therefore, the reduction in turnover rate is likely primarily due to impairment of the product release process. Significantly, the Ψ production at the steady-state phase of multiple-turnover reactions was nearly arrested in Cbf5 mutants R156Q, L145G, and L153G, suggesting that product release is extremely slow in these RNPs.

The activity of Gar1-minus RNP was detectable only in 1 M NaCl, but not in 0.1 M NaCl (data not shown). Generally, other RNPs are also more active at high salt concentrations. The Gar1-minus RNP was extremely defective in multiple-turnover reactions, as shown by a background yield in 20 μM substrate and a low yield (~9%) in 5 μM substrate. The yield in 5 μM substrate was unchanged over time, consistent with a blockage of product release. The activity of Gar1-minus was also substantially weaker than fully assembled RNPs under the single-turnover conditions of 1 and 0.01 μM substrate. Therefore, deletion of Gar1 may compromise substrate loading/catalysis in addition to product release.

The consequences of single-site mutations generally correlate with the role of respective residues in substrate-free or bound RNP structures. The effects of Cbf5 mutations R156Q and Q141N may be due to their destabilization of the closed state, whereas the effects of mutations at the thumb-Gar1 interface (Cbf5 I140G, L145G, and L153G; Gar1 L26A, L26G, and V44D) could be attributed to interference with the open state of the thumb. Kinetic defects in these mutants suggest that both the closed and open states of the thumb are important for substrate turnover. It is also possible that some mutations change the dynamics or transitive states of the enzyme, which would not be captured in static crystal structure. As a notable case, the side chain of R151 is not found in any RNA or protein interaction, but a Gln mutation at this position significantly reduces the rate of substrate turnover.

Active Site and Product

The nucleotide f^5U in our substrate RNA is an unnatural substrate for ΨSs and is often used for probing the chemical mechanism of pseudouridylation (Figure 6A). f^5U can be converted into the hydrolyzed product 5-fluoro-6-hydroxy-pseudouridine ($f^5ho^6\Psi$), as observed in the TruB and RluA structures (Hoang and Ferre-D'Amare, 2001; Hoang et al., 2006). In our structure, the density of the nucleobase at the active site is much weaker than that of nearby atoms (Figure 6B), likely due to X-ray damage (Hoang et al., 2006). One feature of the remaining density indicates that the base is not coplanar with the glycosidic bond and is covalently linked to the ribose, suggesting that the base of f^5U has been rearranged to attach to the ribose via its sp3-hybridized C5 atom. The base was plausibly modeled as

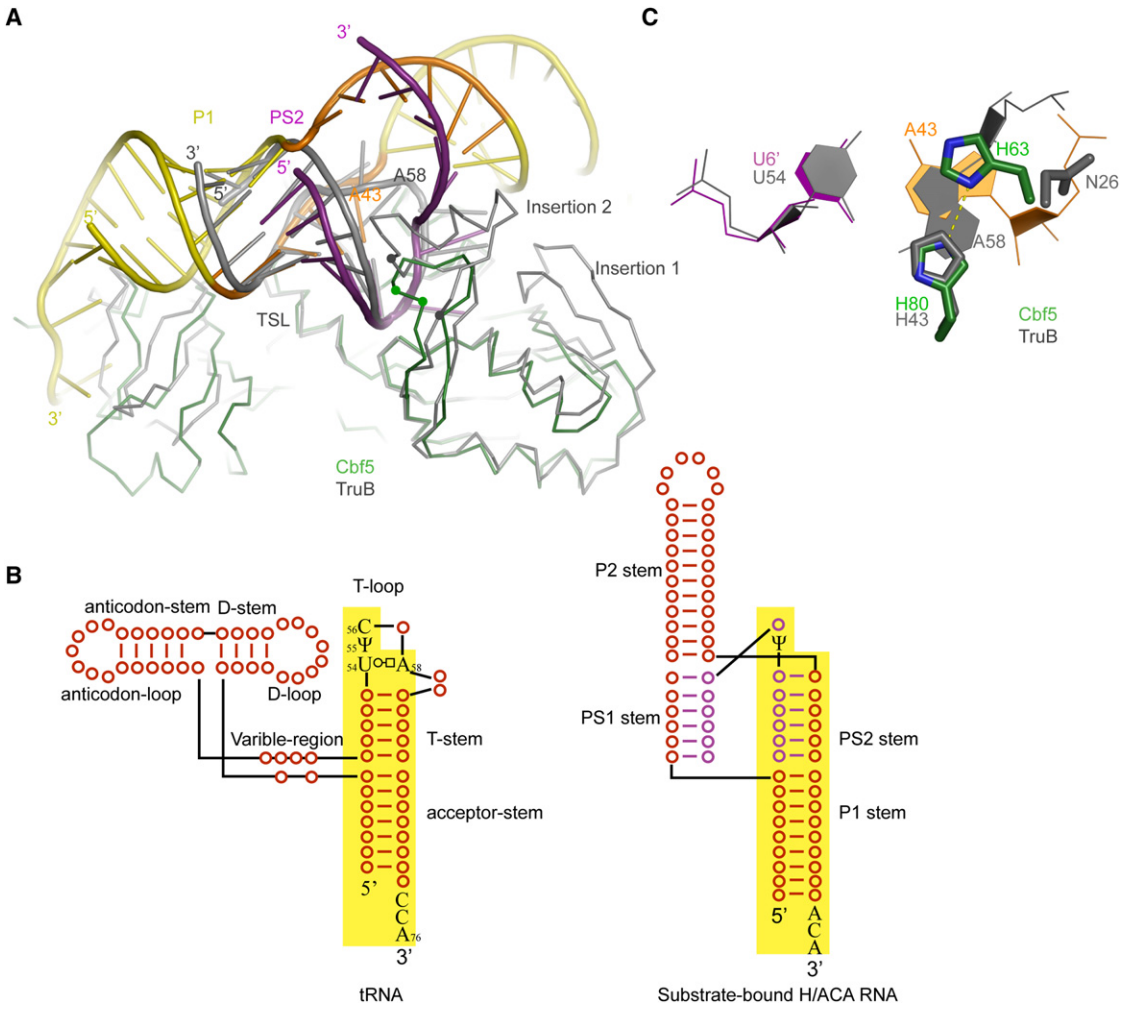

Figure 7. Comparison of Substrate-Bound H/ACA RNP and the TruB-TSL Complex

(A) Structural alignment of substrate-bound H/ACA RNP and TruB-TSL complex. Proteins are shown as Cα traces, and RNAs are shown as ribbons. The H/ACA RNP structure is colored as in Figure 1B, and the TruB-TSL structure is colored in gray. The TruB-specific insertions 1 and 2 are indicated. The boundaries of TruB insertion 2 are marked by gray circles, and the corresponding residues in Cbf5 are marked by green circles.

(B) Correspondence between substrate-bound H/ACA RNA and tRNA. The regions commonly recognized by Cbf5/TruB are shaded in yellow. A canonical tRNA structure is shown in L representation. Nucleotides are shown as red circles or as letters when specifically recognized. The substrate of H/ACA RNA is colored purple.

(C) Different capping interactions at the end of the tRNA T stem and the H/ACA substrate-guide helix PS2.

$f^5ho^6\Psi$. The O6 position is devoid of density, suggesting that O6 was either particularly susceptible to X-ray damage or not properly modeled.

The product $f^5ho^6\Psi$ is buried inside the active site cleft and stabilized by a large number of interactions (Figure 6C). The configuration of the active site and the structure of the product are highly similar to those in TruB (Hoang and Ferre-D'Amare, 2001), suggesting that closed related Cbf5 and TruB follow the same mechanism for pseudouridylation catalysis.

Comparison with TruB-TSL Complex

Though Cbf5 and TruB share similar sequence and structure (Hoang and Ferre-D'Amare, 2001; Hamma et al., 2005; Manival et al., 2006; Rashid et al., 2006), they use two distinct mechanisms to select specific uridine for modification. TruB recognizes the preformed structure of the T stem loop (TSL) of tRNA, whereas Cbf5 in H/ACA RNP relies on guide RNA to recognize its complementary substrate sequence. More recently, archaeal Cbf5 was shown to synthesize Ψ55 of tRNA by itself (Roovers et al., 2006). We compare the structures of the substrate-bound H/ACA RNP and TruB-TSL complex to illustrate structural conservation and adaptation between the RNA-guided and stand-alone ΨS and to understand the recognition of tRNA by Cbf5.

The structure of TruB and Cbf5 in their substrate-bound forms can be aligned with an rmsd of 0.66 Å for 87 Cα atoms (Figure 7A). The most aligned atoms are located exclusively at the catalytic domain and concentrate near the active site cleft,

whereas the peripheral structural elements, including the PUA domain, are more variable. Following the protein alignment, the substrate-guide duplex PS2 superposes well with the tRNA T stem, and the target and its 3′ nucleotide also assume a nearly identical conformation in the two structures. The alignment indicates that Cbf5 and TruB recognize a similar RNA structure composed of a helix and a 2 nt 3′ overhang that contains the target uridine as the first unpaired base in both the substrate-bound H/ACA RNA and tRNA. This observation confirms the previous prediction (Hoang and Ferre-D'Amare, 2001). Moreover, the P1 stem and ACA motif in H/ACA RNA are likely analogous to the acceptor stem and CCA motif of the tRNA, based on their interaction with the PUA domain and their coaxial stacking relationship with the PS2 helix or the T stem (Figure 7B).

The structural similarity between substrate-bound H/ACA RNA and tRNA provides the basis for Cbf5 recognition of tRNA. However, Cbf5 and TruB still exhibit different structural requirements for tRNA (Roovers et al., 2006; Muller et al., 2007; Gurha et al., 2007). TruB minimally requires a T stem loop for recognition, whereas Cbf5 also recognizes the 3′ CCA tail and acceptor stem of tRNA. This is probably because Cbf5 has a more elaborated PUA domain. TruB recognizes a conserved C/U at position 56 (Gu et al., 1998; Becker et al., 1997), but Cbf5 does not (Gurha et al., 2007). The C56 is placed in a size-restricted cavity surrounded by TruB-specific insertion 1 (Hoang and Ferre-D'Amare, 2001). Cbf5 stacks over the corresponding base G8′ in our structure yet does not recognize its sequence or size (Figure 3B). TruB also recognizes the conserved reverse Hoogsteen U54•A58 pair at the end of T stem of tRNA (Gu et al., 1998; Becker et al., 1997), whereas Cbf5 does not (Gurha et al., 2007). The discussion below provides an explanation for this difference.

In the TruB-TLS structure, the U54•A58 reverse Hoogsteen pair is capped at adenine 58 by H43, a residue critical for flipping out the target U55 (Hoang and Ferre-D'Amare, 2001). In H/ACA RNP, the substrate-guide helix PS2 ends with a Watson-Crick pair, the U6′•A43 pair in our structure. U54 and U6′ nearly coincide with each other in the aligned structures (Figure 7C), but A58 and A43 assume markedly different orientations because the glycosidic bonds of U54 and A58 in the reverse Hoogsteen pair are in *trans* orientation relative to the direction of base pairing, whereas the glycosidic bonds in the U6′•A43 Watson-Crick pair are in *cis*. Consequently, H80 in Cbf5, the residue equivalent to H43 in TruB, no longer stacks over A43. Any other base at position 43 would similarly lose the stacking interaction of H80 because of the isosteric structure of the Watson-Crick pair. Interestingly, Cbf5 innovates another histidine at position 63 to stack over A43 (Figures 3A and 7C). Therefore, the T stem and PS2 helix are capped by a different histidine in Cbf5 and TruB, which accounts for the differences in the structure of the terminal base pairs. Both H63 and H80 are invariant in Cbf5 proteins, allowing Cbf5 to recognize both the normal Watson-Crick pair in H/ACA guide-substrate RNA complex and the reverse Hoogsteen pair in tRNA, fulfilling its dual guide-dependent and guide-independent roles. Consistent with the structural role of H80, mutation of H80 has been shown to strongly impair the tRNA activity of Cbf5 but has no effect on its RNA-guided activity (Muller et al., 2007). The presence of H63 would also make Cbf5 to recognize some tRNA substrates without the reverse Hoogsteen pair (Gurha et al., 2007).

The thumb of Cbf5 is missing a 17 residue segment (insertion 2) as compared with TruB (Hoang and Ferre-D'Amare, 2001), which, if present, would insert between residues K150 and R151 of Cbf5. The thumb of Cbf5 otherwise assumes a conformation that strikingly matches its counterpart in TruB. Cbf5 cannot have a TruB-like insertion because the insertion would sterically interfere with the 3′ arm of substrate RNA (Figure 7A). However, the abridged Cbf5 thumb should still be capable of binding the T stem loop of the tRNA without any interference.

The sequence pattern in the matching regions of the Cbf5 and TruB thumb displays strong similarity as well as notable variations, likely reflecting their functional adaptation (Figure 3C). Residues 140 and 153 are more hydrophobic in Cbf5, possibly due to their interaction with Gar1. The Cbf5 thumb is much more basic at positions 142, 146, 151, and 156 than the corresponding residues in TruB, and except for residue R156, these basic residues do not directly contact RNA in the substrate-bound H/ACA RNP structure. They might increase overall electrostatic attraction of the thumb to negatively charged RNA substrate, facilitating substrate association.

In sum, the structural comparison indicates that Cbf5 and TruB not only share homologous sequence and structure, but also recognize a similar structure of RNA near the active site. There are additional prominent changes in the Cbf5 and TruB structure to account for the different structure of their respective substrates. Cbf5 has an elaborated PUA domain, a shortened thumb, and an alternative capping histidine residue for the substrate helix. These structural changes seem to justify the alternative recognition of tRNA structure by Cbf5.

DISCUSSION

In this study, we determined a 2.1 Å structure of substrate-bound H/ACA RNP without Gar1 and a low-resolution structure of substrate-bound RNP with all of its components. Our structures reveal the active conformation of the enzyme with the converted target bound at the active site and ample substrate-Cbf5 interactions and provide important insight into the mechanism of substrate recruitment in H/ACA RNA-guided ΨS.

Our structures show that the substrate associates with the largely preset ψ pocket by forming two specificity-determining substrate-guide helices. The substrate-bound ψ pocket further stacks over the flanking upper and lower stems and interacts with the catalytic domain of Cbf5, eventually leading the target uridine to the active site. The upper and lower stems not only place the guides near the active cleft prior to substrate binding, but also critically coordinate the conformation of loaded substrate because disruption of their positioning in the RNP was detrimental to the activity (Baker et al., 2005; Charpentier et al., 2005; Gurha et al., 2007; Liang et al., 2007, 2008). Interaction with the thumb is also necessary for substrate to adopt a catalytic-competent conformation, as we showed that deletion of the thumb or mutation of a key residue R154 completely abolished the modification. Although the substrate was capable of

binding H/ACA guide RNA in the absence of protein contacts (Jin et al., 2007; Wu and Feigon, 2007; Liang et al., 2007), the substrate-guide complex in those structures cannot be fit into our structure without undergoing significant bending and twisting. Productive substrate recruitment clearly requires correct assembly of the substrate and guide RNA into the RNP complex, in addition to the substrate-guide pairing.

Our activity measurement with excess substrate indicates that H/ACA RNP by itself is a multiple-turnover enzyme. However, the enzyme is slow, with a 0.32 min^{-1} turnover rate at a specified experimental condition. A few putative RNA helicases—Dbp4, Has1, and Rok1—have been implicated in the release of snoRNA from preribosomes (Bohnsack et al., 2008; Liang and Fournier, 2006; Kos and Tollervey, 2005). Interestingly, depletion of these helicases was recently shown to promote the release of nonmodification guide snoRNAs involved in rRNA processing, but this depletion did not affect the dissociation of modification guide snoRNAs (Bohnsack et al., 2008). Substrate release in H/ACA guide RNP might be an autonomous process in vivo, as we demonstrated in vitro. Natural substrates of H/ACA RNP are precursor rRNAs that actively fold and assemble with protein in cells. The folding potential of the substrate might accelerate substrate release in vivo.

Our structures demonstrate that the thumb of Cbf5 plays a critical role in substrate recruitment by pinching the loaded substrate at the active site. When not binding substrate, the thumb could adopt a Gar1-bound open state. Such a state has been shown in the substrate-free RNP structure and in the inactive substrate-bound L7Ae-minus complex (Li and Ye, 2006; Liang et al., 2007). The conformational switch of the thumb between the substrate and Gar1 might be a key step in controlling substrate turnover. With mutagenesis and enzyme kinetics analysis, we found a few single-site mutant RNPs that have a reduced turnover rate in multiple-turnover reactions but appeared to be normal in single-turnover reactions. This observation suggests that product release is inhibited in these mutant RNPs and has become a rate-limiting step. Some mutations are located at the thumb-Gar1 interface (Cbf5 I140G, L145G, and L153G; Gar1 L26A, L26G, and V44D), supporting the notion that the thumb-Gar1 interaction in the open state contributes to product release. The release of product conceivably requires breakage of numerous thumb-substrate RNA interactions. Gar1 might provide a low-energy binding site for the thumb and drive its dissociation from the substrate once modification is completed. Product release was also inhibited in other mutations that destabilize the closed state (Cbf5 R156Q and Q141N) or are not associated with the closed or open state (Cbf5 R151Q), implicating a complex mechanism governing H/ACA RNP kinetics. Moreover, deletion of Gar1 not only blocks substrate release, but also inhibits substrate loading and catalysis, suggesting that Gar1 also contributes to efficient substrate loading and catalysis. Our current analysis is limited by low temporal resolution, which is insufficient to characterize the rapid kinetics at the presteady state. Future studies based on more sophisticated approaches are necessary to understand the precise kinetic process of H/ACA RNA-guided pseudouridylation and its perturbation by mutation.

EXPERIMENTAL PROCEDURES

Protein Expression, Purification, and Crystallization

P. furiosus H/ACA RNP complexes were prepared essentially as previously described (Li and Ye, 2006). The Gar1-minus complex was assembled from RNA1, L7Ae, and the Cbf5-Nop10 subcomplex. The full complex was assembled from RNA2, L7Ae, and the Cbf5-Nop10-Gar1 subcomplex. RNA1, which has 63 nucleotides with the sequence shown in Figure 1A, and RNA2, which contains a 5′-GGCUGCCU-3′ extension at the 5′ end of RNA1, were transcribed from EcoRV-linearized plasmid templates. The Cbf5-Nop10 subcomplex was copurified through Histrap and Heparin chromatography. The substrate with the sequence 5′-AUAAUU(f^5U)GACUCAA-3′ (Dharmacon) was dissolved in water and added to preassembled H/ACA RNPs (60 μM in 5 mM HEPES-Na [pH 7.6]) in a molar ratio of 1.5:1 prior to crystallization. Crystallization was performed at 20°C using the hanging-drop vapor diffusion method. Crystals of the substrate-bound Gar1-minus complex were obtain in 0.2 M ammonium acetate, 0.15 M magnesium acetate, 4% polyethylene glycol (PEG) 8000, and 50 mM cacodylate sodium (pH 6.0) and briefly cryoprotected in the above solution with PEG 8000 replaced by 30% PEG 400 before being flash frozen in liquid nitrogen. Crystals of the substrate-bound full complex were grown in 1.5 M lithium sulfate and 50 mM sodium acetate (pH 4.9) and were cryoprotected with 25% glycerol in the crystallization solution. Diffraction data were collected at 100 K on beamline 3W1A at the Beijing Synchrotron Radiation Facility and on beamline BL41XU at SPring-8, Japan. Data were processed with HKL2000 (Otwinowski and Minor, 1997).

Structural Determination

The structure of the substrate-bound Gar1-minus complex was solved by molecular replacement with the substrate-free H/ACA RNP structure that excluded Gar1, the thumb of Cbf5, and the guide regions of H/ACA RNA as a search model (Li and Ye, 2006). A single copy of the complex was located in the asymmetric unit with the program MOLREP (Vagin and Teplyakov, 1997) in the CCP4 suite (CCP4, 1994). The resulting map clearly showed the density for the RNA and polypeptide missing in the search model. The model was built in COOT (Emsley and Cowtan, 2004) and refined with Refmac (Murshudov et al., 1999). The current model was refined against a 2.1 Å data set and includes Cbf5 (11–339), L7Ae (4–124), Nop10 (3–55), RNA1 (1–25, 28–60), substrate RNA (1–14), 5 PEG molecules, 5 hydrated magnesium ions, and 362 water molecules. The structure of the substrate-bound full complex was solved by molecular replacement, using the above Gar1-minus complex structure as a search model. The resulting map showed density for Gar1 and the 5′ extension of RNA2. The model was refined in Refmac to 5 Å resolution by rigid body refinement and restrained refinement under tight chemical constrains. The full-complex model includes Cbf5 (11–337), L7Ae (4–124), Nop10 (3–55), Gar1 (1–74), RNA2 (−7–60) and substrate RNA (1–14). The numbering of *P. furiosus* Cbf5 has a +3 offset from its sequence in the database to be consistent with the original report of its structure. Structural figures were produced in PyMOL 0.99 (DeLano, 2002).

Mutagenesis and Activity Measurement

The ^{32}P-labeled substrate was generated by ligating a 5′ half RNA (5′-dA dACGGUUAAUUU-3′) and a 5′ end ^{32}P-labeled 3′ half RNA (5′-GACUCAA CACdAdA-3′), as previously described (Li and Ye, 2006; Wang et al., 2002). The resulting product has a single ^{32}P at the 3′ end of the target uridine. Unlabeled substrate RNA has the sequence 5′-AUAAUUUGACUCAA-3′. Mutations in Cbf5 and Gar1 were created by the QuikChange method (Stratagene) using proper primer pairs (see Supplemental Data). In the Cbf5 DEL7 mutant, residues 143–152 were replaced by amino acids Gly-Pro-Gly. All mutant genes were shown by DNA sequencing to be correct, except that the Cbf5 mutant R146Q contains a second E162G mutation. Cbf5 and its mutants were copurified in complex with Nop10, as described above. Gar1 and its mutants were heat treated and purified by Heparin chromatography. H/ACA RNPs were assembled from 10 μM H/ACA RNA1 and stoichiometric amounts of L7Ae, Cbf5-Nop10 subcomplex and Gar1 in 1 M NaCl and 50 mM phosphate buffer (pH 7.0) at 60°C for 30 min. The amounts of L7Ae, Cbf5-Nop10, and Gar1 were adjusted in order, according to the extent of RNP formation in 5% native gel. The pseudouridylation reactions were performed with 1 μM preassembled

H/ACA RNP (referring to the RNA1 concentration), ~10 nM ^{32}P-labeled substrate, and unlabeled substrate of 0, 1, 5, or 20 μM in 1 M NaCl and 50 mM phosphate (pH 7.0). The reactions were incubated at 37°C, and 10 μl aliquots were sampled at 10 and 30 min for 0.01 μM substrate reactions; at 5, 15, and 60 min for 1 and 5 μM substrate reactions; and at 5, 30, 60, and 120 min for 20 μM substrate reactions. After phenol extraction and ethanol precipitation, RNAs were dissolved in 10 μl digestion solution containing 1 mg/ml RNase A, 0.01 U/μl S7 nuclease, 10 mM $CaCl_2$, and 50 mM Tris-HCl (pH 8.0) and were incubated overnight at 37°C. The digested products of 3′-monophosphate nucleotides were loaded onto a cellulose polyethyleneimine plate (Merck), developed in isopropanol-HCl-water (70:15:15 volume ratio) for 2 hr, and quantified by phosphorimaging (Typhoon, GE Healthcare). The fraction of Ψ (y) as a function of time (t) was fit to the function $y = 1 - e^{-At}$, in which A is the rate constant. The rate constant A was multiplied by the substrate-to-enzyme ratio, yielding the turnover rate at time zero.

ACCESSION NUMBERS

Structure factors and coordinates have been deposited in the Protein Data Bank with accession code 3HAX for the substrate-bound Gar1-minus complex and 3HAY for the substrate-bound full complex.

SUPPLEMENTAL DATA

The Supplemental Data include one table and one movie and can be found with this article online at http://www.cell.com/molecular-cell/supplemental/S1097-2765(09)00312-8.

ACKNOWLEDGMENTS

We are grateful to Ning Yan (Tsinghua University), Nobutaka Shimizu, and Masahide Kawamoto for data collection at SPring-8 and to Yuhui Dong, Peng Liu, and Haifeng Hou for data collection at the Beijing Synchrotron Radiation Facility. This work was supported by the Chinese Ministry of Science and Technology and Beijing Municipal Government. J.D. crystallized the substrate-bound Gar-minus complex and carried out biochemical assay. L.L. crystallized the substrate-bound full complex. J.L. and W.W. contributed to biochemical assay. K.Y. solved the X-ray structures and wrote the paper.

Received: January 21, 2009
Revised: April 11, 2009
Accepted: May 7, 2009
Published: May 28, 2009

REFERENCES

Baker, D.L., Youssef, O.A., Chastkofsky, M.I., Dy, D.A., Terns, R.M., and Terns, M.P. (2005). RNA-guided RNA modification: Functional organization of the archaeal H/ACA RNP. Genes Dev. *19*, 1238–1248.

Balakin, A.G., Smith, L., and Fournier, M.J. (1996). The RNA world of the nucleolus: Two major families of small RNAs defined by different box elements with related functions. Cell *86*, 823–834.

Becker, H.F., Motorin, Y., Sissler, M., Florentz, C., and Grosjean, H. (1997). Major identity determinants for enzymatic formation of ribothymidine and pseudouridine in the T psi-loop of yeast tRNAs. J. Mol. Biol. *274*, 505–518.

Bohnsack, M.T., Kos, M., and Tollervey, D. (2008). Quantitative analysis of snoRNA association with pre-ribosomes and release of snR30 by Rok1 helicase. EMBO Rep. *9*, 1230–1236.

Charpentier, B., Muller, S., and Branlant, C. (2005). Reconstitution of archaeal H/ACA small ribonucleoprotein complexes active in pseudouridylation. Nucleic Acids Res. *33*, 3133–3144.

Collaborative Computational Project. (1994). The CCP4 suite: Programs for protein crystallography. Acta Crystallogr. D Biol. Crystallogr. *50*, 760–763.

Crooks, G.E., Hon, G., Chandonia, J.M., and Brenner, S.E. (2004). WebLogo: A sequence logo generator. Genome Res. *14*, 1188–1190.

DeLano, W.L. (2002). The PyMOL user's manual (San Carlos, CA: Delano Scientific).

Ejby, M., Sorensen, M.A., and Pedersen, S. (2007). Pseudouridylation of helix 69 of 23S rRNA is necessary for an effective translation termination. Proc. Natl. Acad. Sci. USA *104*, 19410–19415.

Emsley, P., and Cowtan, K. (2004). Coot: Model-building tools for molecular graphics. Acta Crystallogr. D Biol. Crystallogr. *60*, 2126–2132.

Ganot, P., Bortolin, M.L., and Kiss, T. (1997a). Site-specific pseudouridine formation in preribosomal RNA is guided by small nucleolar RNAs. Cell *89*, 799–809.

Ganot, P., Caizergues-Ferrer, M., and Kiss, T. (1997b). The family of box ACA small nucleolar RNAs is defined by an evolutionarily conserved secondary structure and ubiquitous sequence elements essential for RNA accumulation. Genes Dev. *11*, 941–956.

Gu, X., Yu, M., Ivanetich, K.M., and Santi, D.V. (1998). Molecular recognition of tRNA by tRNA pseudouridine 55 synthase. Biochemistry *37*, 339–343.

Gurha, P., Joardar, A., Chaurasia, P., and Gupta, R. (2007). Differential roles of archaeal box H/ACA proteins in guide RNA-dependent and independent pseudouridine formation. RNA Biol. *4*, 101–109.

Hamma, T., and Ferre-D'Amare, A.R. (2006). Pseudouridine synthases. Chem. Biol. *13*, 1125–1135.

Hamma, T., Reichow, S.L., Varani, G., and Ferre-D'Amare, A.R. (2005). The Cbf5-Nop10 complex is a molecular bracket that organizes box H/ACA RNPs. Nat. Struct. Mol. Biol. *12*, 1101–1107.

Hoang, C., and Ferre-D'Amare, A.R. (2001). Cocrystal structure of a tRNA Psi55 pseudouridine synthase: Nucleotide flipping by an RNA-modifying enzyme. Cell *107*, 929–939.

Hoang, C., Chen, J., Vizthum, C.A., Kandel, J.M., Hamilton, C.S., Mueller, E.G., and Ferre-D'Amare, A.R. (2006). Crystal structure of pseudouridine synthase RluA: Indirect sequence readout through protein-induced RNA structure. Mol. Cell *24*, 535–545.

Hur, S., and Stroud, R.M. (2007). How U38, 39, and 40 of many tRNAs become the targets for pseudouridylation by TruA. Mol. Cell *26*, 189–203.

Jin, H., Loria, J.P., and Moore, P.B. (2007). Solution structure of an rRNA substrate bound to the pseudouridylation pocket of a box H/ACA snoRNA. Mol. Cell *26*, 205–215.

Khanna, M., Wu, H., Johansson, C., Caizergues-Ferrer, M., and Feigon, J. (2006). Structural study of the H/ACA snoRNP components Nop10p and the 3′ hairpin of U65 snoRNA. RNA *12*, 40–52.

King, T.H., Liu, B., McCully, R.R., and Fournier, M.J. (2003). Ribosome structure and activity are altered in cells lacking snoRNPs that form pseudouridines in the peptidyl transferase center. Mol. Cell *11*, 425–435.

Kiss, T. (2001). Small nucleolar RNA-guided post-transcriptional modification of cellular RNAs. EMBO J. *20*, 3617–3622.

Koonin, E.V. (1996). Pseudouridine synthases: Four families of enzymes containing a putative uridine-binding motif also conserved in dUTPases and dCTP deaminases. Nucleic Acids Res. *24*, 2411–2415.

Kos, M., and Tollervey, D. (2005). The putative RNA helicase Dbp4p is required for release of the U14 snoRNA from preribosomes in Saccharomyces cerevisiae. Mol. Cell *20*, 53–64.

Leontis, N.B., and Westhof, E. (2001). Geometric nomenclature and classification of RNA base pairs. RNA *7*, 499–512.

Li, H. (2008). Unveiling substrate RNA binding to H/ACA RNPs: One side fits all. Curr. Opin. Struct. Biol. *18*, 78–85.

Li, L., and Ye, K. (2006). Crystal structure of an H/ACA box ribonucleoprotein particle. Nature *443*, 302–307.

Liang, X.H., and Fournier, M.J. (2006). The helicase Has1p is required for snoRNA release from pre-rRNA. Mol. Cell. Biol. *26*, 7437–7450.

Liang, B., Xue, S., Terns, R.M., Terns, M.P., and Li, H. (2007). Substrate RNA positioning in the archaeal H/ACA ribonucleoprotein complex. Nat. Struct. Mol. Biol. *14*, 1189–1195.

Liang, B., Kahen, E.J., Calvin, K., Zhou, J., Blanco, M., and Li, H. (2008). Long-distance placement of substrate RNA by H/ACA proteins. RNA *14*, 2086–2094.

Manival, X., Charron, C., Fourmann, J.B., Godard, F., Charpentier, B., and Branlant, C. (2006). Crystal structure determination and site-directed mutagenesis of the Pyrococcus abyssi aCBF5-aNOP10 complex reveal crucial roles of the C-terminal domains of both proteins in H/ACA sRNP activity. Nucleic Acids Res. *34*, 826–839.

Meier, U.T. (2005). The many facets of H/ACA ribonucleoproteins. Chromosoma *114*, 1–14.

Muller, S., Fourmann, J.B., Loegler, C., Charpentier, B., and Branlant, C. (2007). Identification of determinants in the protein partners aCBF5 and aNOP10 necessary for the tRNA:Psi55-synthase and RNA-guided RNA: Psi-synthase activities. Nucleic Acids Res. *35*, 5610–5624.

Murshudov, G.N., Vagin, A.A., Lebedev, A., Wilson, K.S., and Dodson, E.J. (1999). Efficient anisotropic refinement of macromolecular structures using FFT. Acta Crystallogr. D Biol. Crystallogr. *55*, 247–255.

Ni, J., Tien, A.L., and Fournier, M.J. (1997). Small nucleolar RNAs direct site-specific synthesis of pseudouridine in ribosomal RNA. Cell *89*, 565–573.

Otwinowski, Z., and Minor, W. (1997). Processing of X-ray diffraction data collected in oscillation mode. Methods Enzymol. *276*, 307–326.

Pan, H., Agarwalla, S., Moustakas, D.T., Finer-Moore, J., and Stroud, R.M. (2003). Structure of tRNA pseudouridine synthase TruB and its RNA complex: RNA recognition through a combination of rigid docking and induced fit. Proc. Natl. Acad. Sci. USA *100*, 12648–12653.

Phannachet, K., and Huang, R.H. (2004). Conformational change of pseudouridine 55 synthase upon its association with RNA substrate. Nucleic Acids Res. *32*, 1422–1429.

Piekna-Przybylska, D., Przybylski, P., Baudin-Baillieu, A., Rousset, J.P., and Fournier, M.J. (2008). Ribosome performance is enhanced by a rich cluster of pseudouridines in the A-site finger region of the large subunit. J. Biol. Chem. *283*, 26026–26036.

Rashid, R., Liang, B., Baker, D.L., Youssef, O.A., He, Y., Phipps, K., Terns, R.M., Terns, M.P., and Li, H. (2006). Crystal structure of a Cbf5-Nop10-Gar1 complex and implications in RNA-guided pseudouridylation and dyskeratosis congenita. Mol. Cell *21*, 249–260.

Reichow, S.L., and Varani, G. (2008). Nop10 is a conserved H/ACA snoRNP molecular adaptor. Biochemistry *47*, 6148–6156.

Reichow, S.L., Hamma, T., Ferre-D'Amare, A.R., and Varani, G. (2007). The structure and function of small nucleolar ribonucleoproteins. Nucleic Acids Res. *35*, 1452–1464.

Roovers, M., Hale, C., Tricot, C., Terns, M.P., Terns, R.M., Grosjean, H., and Droogmans, L. (2006). Formation of the conserved pseudouridine at position 55 in archaeal tRNA. Nucleic Acids Res. *34*, 4293–4301.

Rozhdestvensky, T.S., Tang, T.H., Tchirkova, I.V., Brosius, J., Bachellerie, J.P., and Huttenhofer, A. (2003). Binding of L7Ae protein to the K-turn of archaeal snoRNAs: A shared RNA binding motif for C/D and H/ACA box snoRNAs in Archaea. Nucleic Acids Res. *31*, 869–877.

Tang, T.H., Bachellerie, J.P., Rozhdestvensky, T., Bortolin, M.L., Huber, H., Drungowski, M., Elge, T., Brosius, J., and Huttenhofer, A. (2002). Identification of 86 candidates for small non-messenger RNAs from the archaeon Archaeoglobus fulgidus. Proc. Natl. Acad. Sci. USA *99*, 7536–7541.

Vagin, A.A., and Teplyakov, A. (1997). MOLREP: An automated program for molecular replacement. J. Appl. Cryst. *30*, 1022–1025.

Wang, C., Query, C.C., and Meier, U.T. (2002). Immunopurified small nucleolar ribonucleoprotein particles pseudouridylate rRNA independently of their association with phosphorylated Nopp140. Mol. Cell. Biol. *22*, 8457–8466.

Wedekind, J.E., and McKay, D.B. (2000). Purification, crystallization, and X-ray diffraction analysis of small ribozymes. Methods Enzymol. *317*, 149–168.

Wu, H., and Feigon, J. (2007). H/ACA small nucleolar RNA pseudouridylation pockets bind substrate RNA to form three-way junctions that position the target U for modification. Proc. Natl. Acad. Sci. USA *104*, 6655–6660.

Yang, C., McPheeters, D.S., and Yu, Y.T. (2005). Psi35 in the branch site recognition region of U2 small nuclear RNA is important for pre-mRNA splicing in Saccharomyces cerevisiae. J. Biol. Chem. *280*, 6655–6662.

Ye, K. (2007). H/ACA guide RNAs, proteins and complexes. Curr. Opin. Struct. Biol. *17*, 287–292.

Yu, Y.T., Shu, M.D., and Steitz, J.A. (1998). Modifications of U2 snRNA are required for snRNP assembly and pre-mRNA splicing. EMBO J. *17*, 5783–5795.